Safety and efficacy of a novel 3D-printed bioresorbable sirolimus-eluting scaffold in a porcine model

Qiuping Shi[1], MD; Bin Zhang[1], PhD, MD; Xingang Wang[1], MD; Jintao Fei[1], MD; Qiao Qin[1], MD; Bo Zheng[1,2]*, MD; Ming Chen[1], MD

1. Department of Cardiology, Peking University First Hospital, Beijing, People's Republic of China; 2. Institute of Cardiovascular Disease, Peking University First Hospital, Beijing, People's Republic of China

Q. Shi and B. Zhang contributed equally to this manuscript.

Abstract

Background: The effect of 3D-printed bioresorbable vascular scaffolds (BRS) in coronary heart disease has not been clarified.

Aims: We aimed to compare the safety and efficacy of 3D-printed BRS with that of metallic sirolimus-eluting stents (SES).

Methods: Thirty-two BRS and 32 SES were implanted into 64 porcine coronary arteries. Quantitative coronary angiography (QCA) and optical coherence tomography (OCT) were performed at 14, 28, 97, and 189 days post-implantation. Scanning electron microscopy (SEM) and histopathological analyses were performed at each assessment.

Results: All stents/scaffolds were successfully implanted. All animals survived for the duration of the study. QCA showed the two devices had a similar stent/scaffold-to-artery ratio and acute percent recoil. OCT showed the lumen area (LA) and scaffold/stent area (SA) of the BRS were significantly smaller than those of the SES at 14 and 28 days post-implantation (14-day LA: BRS vs SES 4.52 ± 0.41 mm^2 vs 5.69 ± 1.11 mm^2; p=0.03; 14-day SA: BRS vs SES 4.99 ± 0.45 mm^2 vs 6.11 ± 1.06 mm^2; p=0.03; 28-day LA: BRS vs SES 2.93 ± 1.03 mm^2 vs 4.82 ± 0.74 mm^2; p=0.003; 28-day SA: BRS vs SES 3.86 ± 0.98 mm^2 vs 5.75 ± 0.71 mm^2; p=0.03). Both the LA and SA of the BRS increased over time and were similar to those of the SES at the 97-day and 189-day assessments. SEM and histomorphological analyses showed no significant between-group differences in endothelialisation at each assessment.

Conclusions: The novel 3D-printed BRS showed safety and efficacy similar to that of SES in a porcine model. The BRS also showed a long-term positive remodelling effect.

---

*Corresponding author: Department of Cardiology, Institute of Cardiovascular Disease, Peking University First Hospital, No.8 Xishiku Str, Xicheng District, Beijing 100034, People's Republic of China. E-mail: zhengbopatrick@163.com

---

Abbreviations

3D	three-dimensional
BRS	bioresorbable vascular scaffold
CHD	coronary heart disease
DES	drug-eluting stent
LA	lumen area
MLD	minimal lumen diameter
NA	neointimal area
OCT	optical coherence tomography
PCI	percutaneous coronary intervention
QCA	quantitative coronary angiography
SA	scaffold/stent area
SEM	scanning electron microscopy
SES	sirolimus-eluting stent
ST	stent thrombosis

Introduction

The development of percutaneous coronary intervention (PCI) has improved the prognosis of patients with coronary heart disease (CHD). However, a permanent metallic implant may contribute to late/very-late stent thrombosis (ST). A bioresorbable vascular scaffold (BRS) has potential advantages over traditional metallic drug-eluting stents (DES), including removal of the rigid caging in the stented vessel and restoring the vessel to a physiological state[1,2]. Owing to its potential biodegradability, a BRS can theoretically reduce late/very-late ST[3]. However, recent studies have revealed an increased incidence of ST and in-stent restenosis following implantation of BRS[4,5]. There are several possible mechanical causes of ST, including malapposition, incomplete coverage of lesions, device-vessel mismatch, stent fracture, late stent discontinuity, stent overlap, uncovered struts, and neoatherosclerosis[6]. Procedural and lesion characteristics are crucial factors, and most of the above-mentioned factors are also possibly related to the scaffold design.

To compensate for the reduced radial strength of non-metallic struts, a BRS requires an appropriate strut thickness. However, thicker struts impede the healing process and increase the risk of malapposition because of factors such as fracture or breaks in the integrity of the BRS as a result of the absorption of the scaffold[7]. Furthermore, the rectangular-shaped struts most often used in the current BRS may affect the local haemodynamic microenvironment in treated vessels and increase the risk of ST[8]. Therefore, there is a need for a re-engineering of the scaffold, including consideration of the type of polymer, the geometric shape and thickness of the strut, and vessel wall coverage.

As is well-known, depending on the characteristics of coronary artery anatomy, tapered coronary artery lesions are often encountered in clinical practice[9] and subsequent stent edge dissection is a predictor of an adverse clinical outcome[10,11]. Due to differences in materials, the current BRS devices cannot be overexpanded in the same way as metal stents and may have an increased risk of proximal malapposition, distal dissection, and haematoma when used in vessels that are obviously tapered. Using 3D printing technology

combined with angiographic image processing, reconstruction, and an innovative fabrication strategy, personalised stents can be produced, thus allowing the production of stents that are more suitable for these lesions. The aim of this preclinical study was to evaluate the safety and efficacy of a novel 3D-printed bioresorbable sirolimus-eluting scaffold with circular-shaped struts and a nanoparticle coating with a fixed size in a normal porcine coronary artery.

Methods

STUDY SCAFFOLDS

The BRS used in this study was the AMSorb (Beijing Advanced Medical Technologies) and the metallic SES used was the HELIOS (Kinhely Medical). The BRS is a 3D-printed balloon-expandable coronary scaffold, which consists of a polymer backbone of novel poly-L-lactic acid (PLLA) coated with a thin layer of a 1:1 mixture of an amorphous matrix of poly(D,L-lactic acid) and 100 $\mu g/cm^2$ of the antiproliferative drug sirolimus. The struts have a cross-sectional circular shape with a thickness of 140 μm **(Figure 1, Table 1)**. The SES consists of an L605 cobalt chromium alloy platform with a thickness of 80 μm coated with a layer of sirolimus (135 $\mu g/cm^2$) with poly(lactic-co-glycolic acid) (PLGA). The scaffold/stent size was fixed for the purposes of this study at 3 mm in diameter and 12 mm in length for both the BRS and SES.
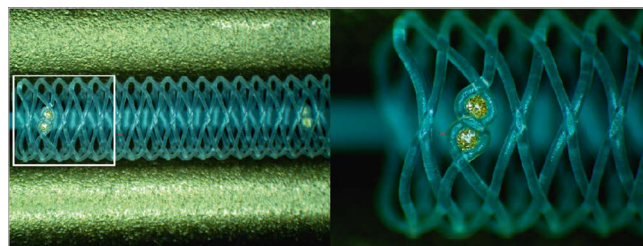

Figure 1. *Configuration and structure of the AMSorb scaffold.*

ANIMALS

The study protocol was approved by the Institutional Animal Care and Use Committee of Peking University First Hospital (reference number J201612) and conducted in accordance with the National Institutes of Health Guide for the Care and Use of Laboratory Animals. Pigs of either sex (weight: 25-40 kg; age: 6-8 months) were sourced from the China Agricultural University and fed a standard laboratory chow diet without added lipids.

EXPERIMENT GROUPS AND PROCEDURE

All animals received pretreatment with 300 mg of aspirin and 75 mg of clopidogrel one day prior to the implantation of the allocated device. Aspirin 100 mg/day and clopidogrel 75 mg/day were administered through to the time each animal was euthanised. A BRS or SES was implanted into either the left anterior descending artery, left circumflex artery, or right coronary artery in

Table 1. Different scaffold of Absorb BRS and AMSorb.

Device	Shape	Backbone	Coating	Drug	Dose	Strut thickness
Absorb BRS	Rounded rectangle	PLLA	PDLLA	Everolimus	100 µg/cm^2	157 µm
AMSorb	Ellipse	PLLA	PDLLA	Sirolimus	100 µg/cm^2	140 µm
BRS: bioresorbable vascular scaffold; PLLA: poly-L-lactic acid; PDLLA: poly(D,L-lactide)						

a randomised manner, so that two types of devices were implanted in two different coronary arteries in each animal **(Table 2)**. The stent/scaffold-to-artery ratio was limited to 1.1-1.2:1 according to the quantitative coronary angiography (QCA) analysis. The method used to induce anaesthesia and the SES implantation procedure have been described previously[12]. The BRS needed to be in contact with blood for more than 90 seconds before delivery to the target coronary segment and then inflated at a steady rate over 10 seconds until it expanded to its maximum diameter. The expansion pressure (generally 8-10 atm) was then maintained for up to 30 seconds. Angiography was repeated after implantation to confirm that no obvious dissection or thrombosis had occurred.

EVALUATION BY QUANTITATIVE CORONARY ANGIOGRAPHY

QCA was performed in eight animals at 14, 28, 97, and 189 days after implantation using CAAS 5.9 QCA software (Pie Medical Imaging). In each vessel, the stent/scaffold segment and the peri-stent/scaffold segment (defined as 5 mm proximal and distal to the stent/scaffold edge) were evaluated post-implantation and at each assessment time. The evaluations were performed independently by two cardiovascular experts (XG. Wang and B. Zhang). A third investigator (B. Zheng) checked their results. The following QCA parameters were measured: minimal lumen diameter (MLD) immediately after implantation, reference vessel diameter, MLD at the various assessment times, percentage diameter stenosis, and late lumen loss (defined as the difference between the MLD post-implantation and the MLD at the assessments post-implantation). We also evaluated acute recoil, which was defined as the difference between the mean diameter of the inflated balloon (X) and the mean lumen diameter of the stent immediately after deflation of the balloon (Y). Acute percent recoil was defined as (X-Y)/X and expressed as a percentage[13].

OPTICAL COHERENCE TOMOGRAPHY IMAGING AND EVALUATION

Optical coherence tomography (OCT) was performed at each assessment using a C7XR Dragonfly imaging system (Abbott) with a pullback speed of 2.5 cm/s (n=8 in each group). The OCT measurements were repeated offline using the LightLab Imaging workstation (Abbott). The OCT evaluations were performed independently by two cardiovascular experts (XG. Wang and B. Zhang). A third investigator (B. Zheng) checked their results. Contiguous cross-sections were analysed at 1 mm longitudinal intervals within the treated segment and at 5 mm proximal and distal to the stent/scaffold edges to measure the proximal and distal reference vessel areas (RVA). The RVA, lumen area (LA), stent/ scaffold area (SA), neointimal area (NA), and percentage area of stenosis were calculated according to the methods used in previous studies[14].

STENT/SCAFFOLD HARVEST AND EVALUATION OF HISTOLOGY AND MORPHOLOGY

Eight animals were euthanised after the imaging examination at each assessment time. Their hearts were removed and perfused with heparinised saline for 30 minutes at a pressure of 100 mmHg (1 mmHg=0.0133 kPa).

For histological and morphological evaluation, the stent/scaffold vessel segment was separated rapidly, fixed in 10% formaldehyde solution, and stained with haematoxylin and eosin for histopathological analysis. The following parameters were investigated according to published methods[15,16]: LA, internal elastic lamina area (IELA), NA (IELA – LA), and percent area of stenosis (IELA – LA/LA×100%) with morphological analysis of injury, inflammation, and endothelialisation.

For scanning electron microscopy (SEM), the stented vessel segments were separated, cut along the longitudinal axis, and fixed with 3% buffered glutaraldehyde and 1% buffered osmium tetroxide (n=2 for SES, n=2 for BRS). The samples were then dehydrated in a series of ethanol baths (50%, 75% and 100%), dried in liquid CO_2 in a critical point dryer (72.8 atm, 31°C), and sputter-coated for 3 min at 15 mA with gold. SEM images (H-450; Hitachi) were acquired at low magnification (×18) to evaluate the overall neointimal coverage of the stents and at various high magnifications to identify the composition of the tissue covering the surfaces of the stents. Endothelial cells were identified as sheets of closely connected monolayer cells with a spindle or polygonal shape.

Table 2. Distribution of stents in the coronary arteries at the four assessment times.

	14 days			28 days			97 days			189 days		
	LAD	LCx	RCA	LAD	LCx	RCA	LAD	LCx	RCA	LAD	LCx	RCA
BRS	5	3	0	7	1	0	8	0	0	4	3	1
SES	3	5	0	1	4	3	0	8	0	4	3	1
BRS: bioresorbable sirolimus-eluting scaffold (AMSorb); LAD: left anterior descending artery; LCx: left circumflex artery; RCA: right coronary artery; SES: metallic sirolimus-eluting stent												

STATISTICAL ANALYSIS

Continuous values that were distributed normally are expressed as the mean±standard deviation. Categorical data are expressed as the percentage. *n* represents the number of stents of each type. The independent two-sample t-test was used to detect between-group differences. All statistical analyses of numerical data were performed using SPSS Statistics 24.0 (IBM). A p-value <0.05 was considered statistically significant.

Results

A total of 64 stents/scaffolds (BRS n=32, SES n=32) were successfully implanted in the coronary arteries of 32 pigs. All animals survived for the planned study duration without any complications (angiographic stent thrombosis, migration, or fragmentation).

QUANTITATIVE CORONARY ANGIOGRAPHY ANALYSIS

The results of the QCA analysis at baseline and parameters associated with acute recoil are presented in **Table 3**. There was no difference in the diameter of the reference vessel between the BRS and the SES (2.82±0.32 mm vs 2.76±0.28 mm; p=0.44)

at baseline. The stent-to-artery ratio for the BRS was similar to that for the SES (1.03±0.10 vs 1.07±0.10; p=0.13). The acute absolute recoil was similar in both groups (0.07±0.21 mm vs 0.08±0.17 mm; p=0.98), as was the acute percent recoil (2.50±7.33% vs 2.44±5.78%; p=0.97). The results for MLD immediately after the procedure, MLD at the various assessment times, late lumen loss, and percent diameter of stenosis are presented in **Table 4**. The MLD was significantly smaller for the BRS than for the SES at day 14 (1.90±0.30 mm vs 2.38±0.33 mm; p=0.01) but not at any other assessment time. The late lumen loss and percent diameter of stenosis were comparable between the two groups at each assessment time. The greatest late lumen loss with the BRS was 0.89±0.40 mm at 28 days and with the SES was 0.80±0.31 mm at 97 days.

ANALYSIS BY OPTICAL COHERENCE TOMOGRAPHY

OCT examination was performed successfully for all of the study devices **(Table 5)**. The appearance of the struts at each OCT examination is shown in **Figure 2**. All struts had a preserved box-like appearance with no ST, malapposition, dissection, or tissue

Table 3. QCA analysis at baseline and parameters associated with acute recoil.

Parameter	BRS (n=32)	SES (n=32)	*p*-value
Reference vessel diameter (mm)	2.82±0.32	2.76±0.28	0.44
Stent-to-artery ratio	1.03±0.10	1.07±0.10	0.13
Mean diameter of inflated balloon (X, mm)	2.87±0.13	2.93±0.18	0.15
Mean diameter of stent immediately after balloon inflation (Y, mm)	2.79±0.22	2.85±0.20	0.29
Acute absolute recoil (X-Y, mm)	0.07±0.21	0.08±0.17	0.98
Acute percent recoil ([X-Y]/X, %)	2.50±7.33	2.44±5.78	0.97
BRS: bioresorbable sirolimus-eluting scaffold (AMSorb); QCA: quantitative coronary angiography; SES: metallic sirolimus-eluting stent			

Table 4. QCA analysis of late lumen loss and percentage diameter of stenosis.

14 days	IMLD (mm)	FU-MLD (mm)	LLL (mm)	%DS (%)
BRS (n=8)	2.37±0.11	1.90±0.30	0.47±0.31	19.88±13.36
SES (n=8)	2.62±0.16	2.38±0.33	0.25±0.28	9.33±10.59
p-value	0.002*	0.01*	0.15	0.10
28 days	**IMLD (mm)**	**FU-MLD (mm)**	**LLL (mm)**	**%DS (%)**
BRS (n=8)	2.67±0.28	1.78±0.29	0.89±0.40	32.62±13.26
SES (n=8)	2.66±0.20	2.17±0.45	0.49±0.39	18.54±14.89
p-value	0.94	0.08	0.08	0.09
97 days	**IMLD (mm)**	**FU-MLD (mm)**	**LLL (mm)**	**%DS (%)**
BRS (n=8)	2.57±0.18	1.99±0.20	0.58±0.17	22.56±6.51
SES (n=8)	2.66±0.25	1.85±0.36	0.80±0.31	30.31±11.87
p-value	0.44	0.37	0.10	0.13
189 days	**IMLD (mm)**	**FU-MLD (mm)**	**LLL (mm)**	**%DS (%)**
BRS (n=8)	2.66±0.16	2.17±0.47	0.49±0.51	17.89±18.75
SES (n=8)	2.72±0.19	2.05±0.25	0.67±0.13	24.91±4.37
p-value	0.52	0.51	0.35	0.33
*Statistically significant difference. FU-MLD: MLD at the various assessment times; IMLD: minimal lumen diameter immediately after implantation; LLL: late lumen loss; %DS: percentage of diameter stenosis				

Table 5. OCT analysis at each assessment of the BRS and SES.

14 days	BRS n=8	SES n=8	*p*-value
RVA (mm^2)	5.72±1.30	5.62±1.14	0.88
LA (mm^2)	4.52±0.41	5.69±1.11	0.03*
SA (mm^2)	4.99±0.45	6.11±1.06	0.03*
NA (mm^2)	0.46±0.10	0.43±0.16	0.58
%AS	9.35±1.65	7.28±3.30	0.14
28 days	**n=8**	**n=8**	***p*-value**
RVA (mm^2)	6.06±1.03	5.15±0.7	0.10
LA (mm^2)	2.93±1.03	4.82±0.74	0.003*
SA (mm^2)	3.86±0.98	5.75±0.71	0.002*
NA (mm^2)	0.93±0.39	0.92±0.25	0.98
%AS	25.43±13.21	16.50±4.68	0.15
97 days	**n=8**	**n=8**	***p*-value**
RVA (mm^2)	5.92±0.35	5.62±0.59	0.27
LA (mm^2)	3.90±0.60	3.63±1.08	0.57
SA (mm^2)	5.33±0.83	5.30±0.78	0.93
NA (mm^2)	1.44±0.69	1.67±0.64	0.53
%AS	26.95±9.50	32.43±13.30	0.39
189 days	**n=8**	**n=8**	***p*-value**
RVA (mm^2)	6.65±0.68	6.21±1.36	0.46
LA (mm^2)	4.31±1.06	3.78±0.54	0.32
SA (mm^2)	5.89±1.22	5.54±0.66	0.58
NA (mm^2)	1.58±0.40	1.78±0.56	0.49
%AS	27.22±6.10	31.72±8.07	0.28

*Statistically significant difference. %AS: percentage area of stenosis; BRS: bioresorbable sirolimus-eluting scaffold (AMSorb); LA: lumen area; NA: neointimal area; RVA: reference vessel area; SA: stent area; SES: metallic sirolimus-eluting stent

prolapse in either group. The RVA was similar between the two groups at all assessment times. The LA of the BRS was significantly smaller than that of the SES at 14 days (4.52±0.41 mm^2 vs 5.69±1.11 mm^2; p=0.03) and 28 days (2.93±1.03 mm^2 vs 4.82±0.74 mm^2; p=0.003). The SA showed a pattern similar to that of the LA. The SA of the BRS was significantly smaller than that of the SES at 14 days (4.99±0.45 mm^2 vs 6.11±1.06 mm^2; p=0.03) and 28 days (3.86±0.98 mm^2 vs 5.75±0.71 mm^2; p=0.002). The LA and SA of the BRS were numerically larger than those of the SES at 97 days and 189 days, but the differences were not statistically significant **(Figure 3)**. There was no significant difference in NA or the percent area of stenosis between the BRS and SES at any assessment time.

HISTOPATHOLOGICAL AND HISTOMORPHOLOGICAL ANALYSES

The histopathological findings under light microscopy at each assessment time are shown in **Figure 4** (low magnification, 20×) and **Figure 5** (high magnification, 200×). At each assessment, all BRS and SES devices were structurally intact and all stent/scaffold beam surfaces were covered with endothelial cells. No thrombus formation was observed in either group. The results of the morphological analyses are shown in **Table 6**. There were no statistically significant between-group differences in LA, IELA, NA, or percentage area of stenosis at any assessment time. There were also no significant differences in the injury, inflammation, or endothelialisation scores between the two groups at any assessment **(Table 7)**. The endothelialisation scores were similar between the two groups and showed complete re-endothelialisation at 97 days and 189 days, which is consistent with the findings on SEM **(Figure 6, Figure 7)**.
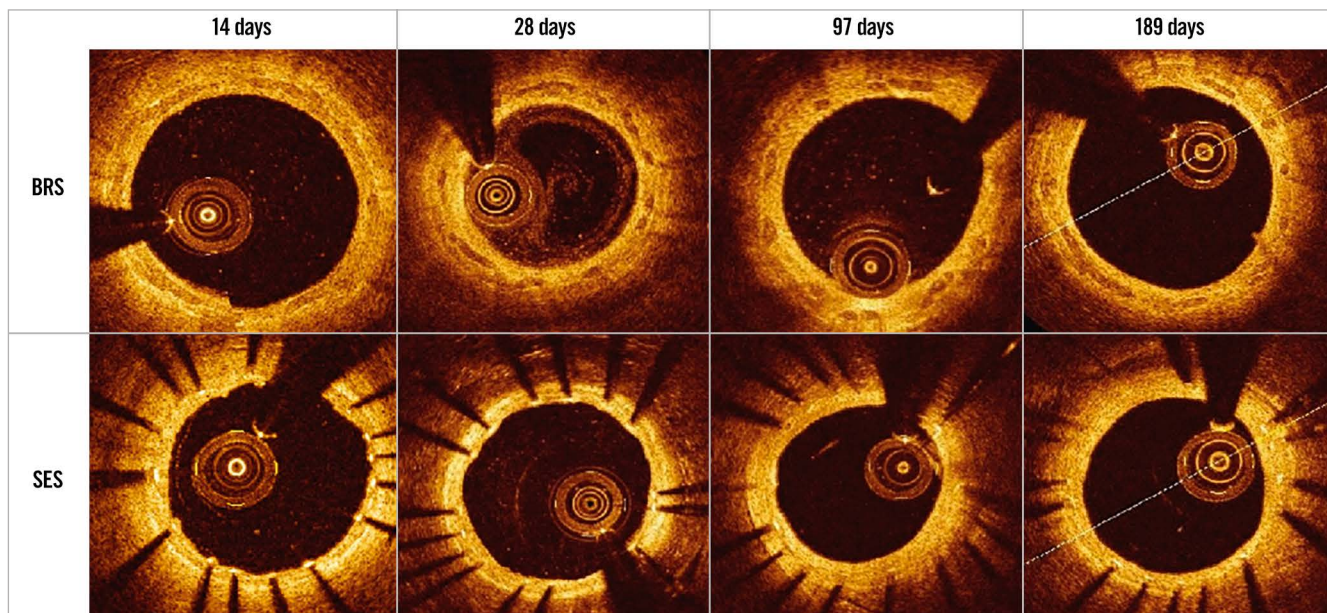

Figure 2. *Performance of the BRS and SES at each optical coherence tomography assessment. BRS: bioresorbable sirolimus-eluting scaffold (AMSorb); SES: metallic sirolimus-eluting stent*
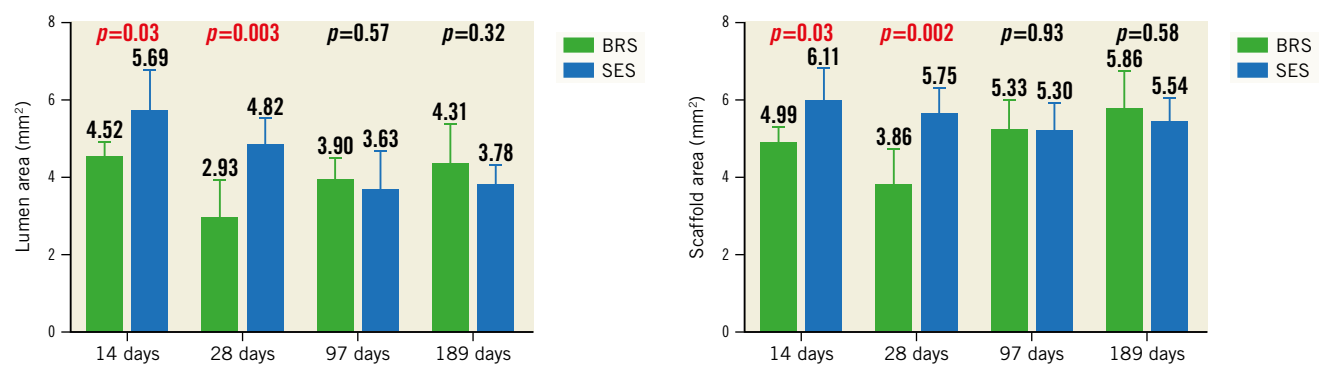
Figure 3. *Lumen area and scaffold/stent area of the BRS and SES at each assessment time. BRS: bioresorbable sirolimus-eluting scaffold (AMSorb); SES: metallic sirolimus-eluting stent*
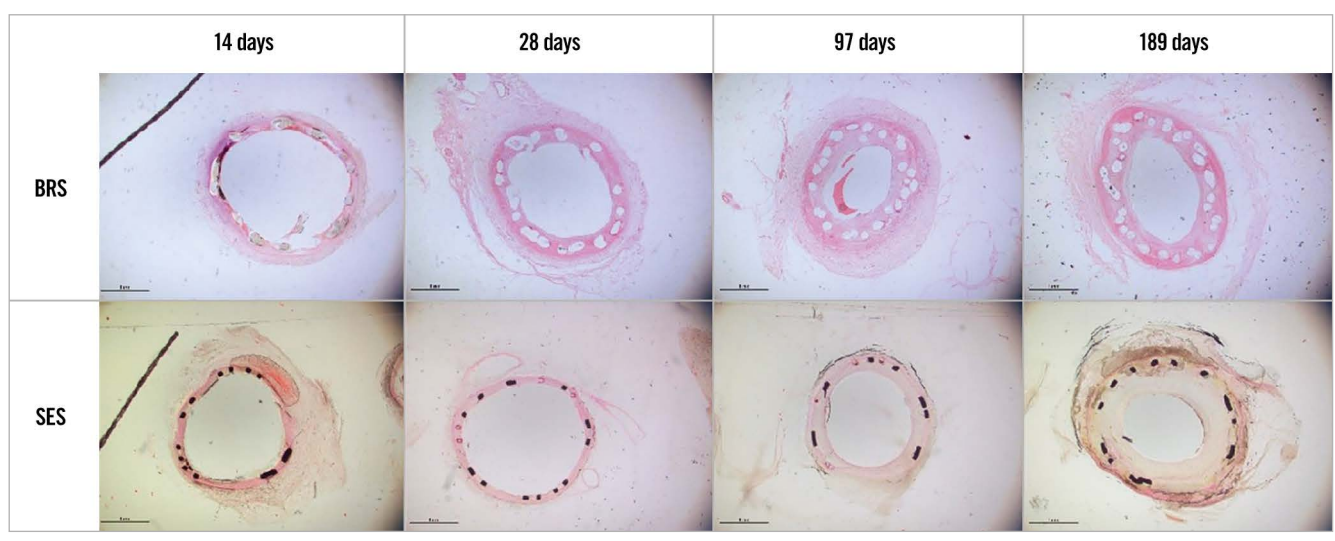

Figure 4. *Histopathological findings for the BRS and SES at each assessment time (low magnification). BRS: bioresorbable sirolimus-eluting scaffold (AMSorb); SES: metallic sirolimus-eluting stent*
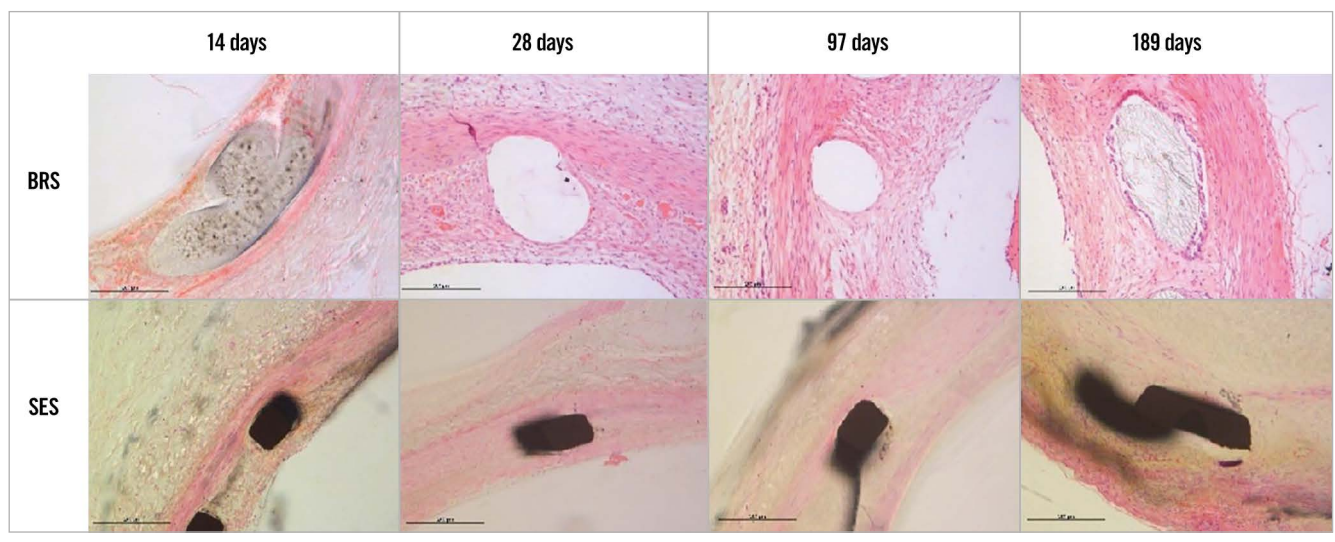

Figure 5. *Histopathological findings for the BRS and SES at each assessment time (high magnification). BRS: bioresorbable sirolimus-eluting scaffold (AMSorb); SES: metallic sirolimus-eluting stent*

**Table 6. Histomorphometric parameters for BRS and SES at each assessment time.**

	14 days		28 days		97 days		189 days	
	BRS n=6	SES n=6	BRS n=6	SES n=6	BRS n=6	SES n=6	BRS n=6	SES n=6
LA (mm^2)	4.16±1.16	4.24±1.56	2.04±1.27	3.18±1.17	1.49±0.61	2.29±1.27	1.96±0.96	2.78±0.92
p-value	0.92		0.14		0.19		0.17	
IELA (mm^2)	4.77±1.20	5.28±1.31	3.58±1.39	4.91±1.07	5.16±2.77	5.31±0.90	4.99±1.35	6.50±1.82
p-value	0.50		0.09		0.90		0.13	
NA (mm^2)	0.61±0.20	1.04±0.85	1.54±0.28	1.73±1.22	3.67±3.29	3.02±1.27	3.03±1.83	3.73±2.36
p-value	0.28		0.73		0.66		0.58	
%AS	13.52±6.02	20.03±15.79	49.09±21.72	34.72±20.44	62.80±20.05	57.26±23.07	57.64±19.49	53.58±20.45
p-value	0.37		0.27		0.67		0.73	

%AS: percentage area of stenosis; BRS: bioresorbable sirolimus-eluting scaffold (AMSorb); LA: lumen area; IELA: internal elastic lamina area; NA: neointimal area; SES: metallic sirolimus-eluting stent

Table 7. Pathological scores for BRS and SES at each assessment time.

	14 days		28 days		97 days		189 days	
	BRS n=6	SES n=6	BRS n=6	SES n=6	BRS n=6	SES n=6	BRS n=6	SES n=6
Inflammation score	0.33±0.52	0.00±0.00	0.50±0.55	0.00±0.00	1.50±1.22	1.17±1.17	1.50±1.05	1.17±1.17
p-value	0.18		0.08		0.64		0.62	
Injury score	0.33±0.52	0.17±0.41	0.33±0.52	0.00±0.00	1.00±1.10	1.00±1.10	0.67±0.82	0.33±0.52
p-value	0.55		0.18		1.00		0.42	
Endothelialisation score	2.17±0.98	2.50±0.84	2.83±0.41	3.00±0.00	3.00±0.00	3.00±0.00	3.00±0.00	3.00±0.00
p-value	0.54		0.36		-		-	

BRS: bioresorbable sirolimus-eluting scaffold (AMSorb); SES: metallic sirolimus-eluting stent
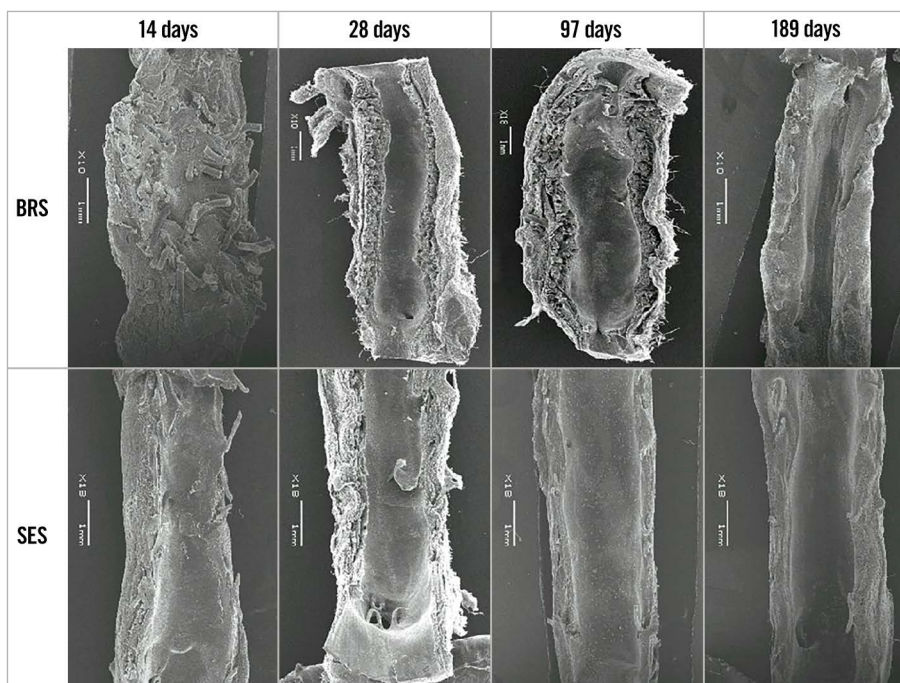
Figure 6. *Findings on scanning electron microscopy for the BRS and SES at each assessment time (low magnification). BRS: bioresorbable sirolimus-eluting scaffold (AMSorb); SES: metallic sirolimus-eluting stent*
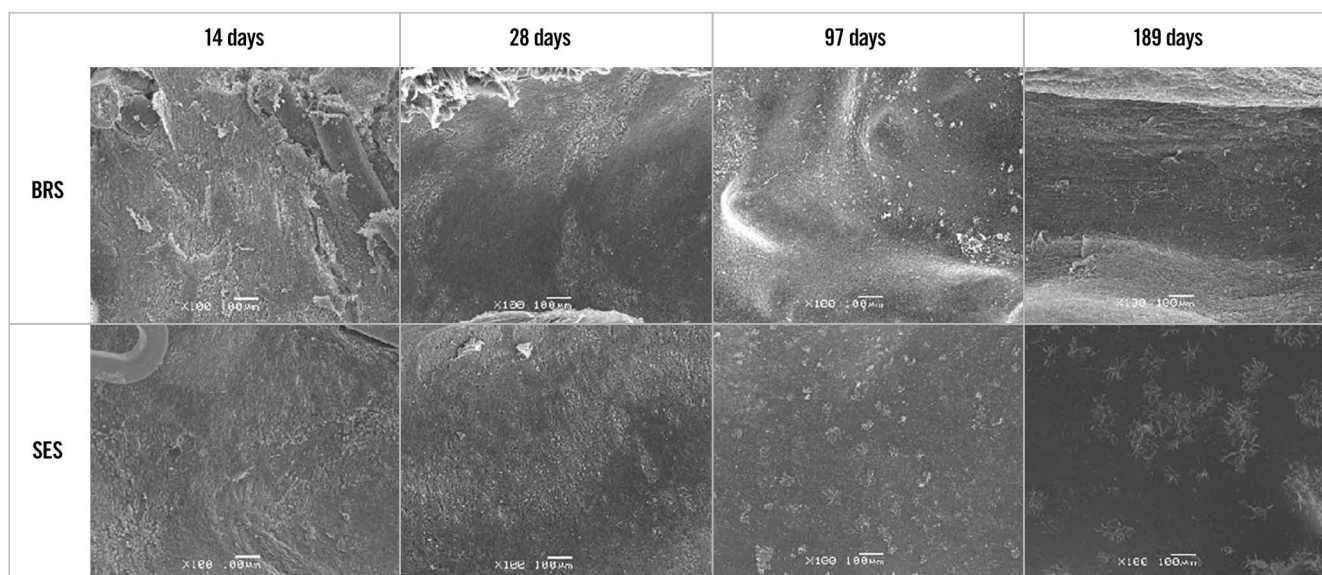
Figure 7. *Findings on scanning electron microscopy for the BRS and SES at each assessment time (high magnification). BRS: bioresorbable sirolimus-eluting scaffold (AMSorb); SES: metallic sirolimus-eluting stent*

Discussion

3D printing technology is gradually being applied in several fields of medicine, including fabrication of medical devices, advanced visualisation, diagnosis planning, and simulation of surgical procedures[17]. However, few systematic long-term studies have demonstrated the feasibility of 3D-printed scaffolds for CHD *in vivo*[18]. This preclinical study further validated the safety of a fully degradable sirolimus-eluting 3D-printed scaffold by implanting it into normal coronary arteries in a porcine model. All animals survived for the entire duration of the study without stent thrombosis, migration, or fragmentation, confirming that the safety of the BRS is comparable with that of the SES. Previous studies have demonstrated the good biocompatibility of the PLLA bioabsorbable vascular stent (BVS)[19,20]. In our histopathological analysis, there were no or few aggregations of inflammatory cells in the BRS-stented arterial wall tissue, which suggests that this stent has favourable biocompatibility. Moreover, it was noted to be inert and non-thrombogenic at the 189-day assessment. In terms of inflammation scores, the BRS seems to be better than BVS in previous studies[15]. The circular shape and smaller thickness of the BRS may be one of the reasons for less inflammation, and the unstable injury score may be another confounding factor. A healthy, intact, and functioning endothelial layer controls thrombosis and thrombolysis, interactions between platelets and leukocytes, and the release of vasodilating (e.g., nitric oxide) and vasoconstricting (e.g., endothelin-1) substances, as well as regulating vascular tone and growth[21]. Early re-endothelialisation would be helpful for suppressing neointimal hyperplasia, preventing restenosis, and reducing complications of ST[22]. Our OCT and SEM analyses showed that the BRS scaffolds had a good degree of endothelial cell coverage at each assessment time. Pathological analysis showed that the endothelialisation scores were similar for the two stents; the BRS achieved early re-endothelialisation within 28 days and complete endothelialisation at 97 days, suggesting that, unlike the SES, the BRS does not delay the re-endothelialisation process. Two-stage degradation and the vascular characteristics of the novel 3D-printed scaffold may demonstrate the potential of this device to promote endothelial function[23].

A bioabsorbable PLLA stent has several advantages due to its good biocompatibility and ability to be moulded into scaffolds of different shapes[19,20]. However, there is still a concern about the acute stent recoil and radial strength of the scaffold because it has material and structural characteristics that are different from those of the metallic stent. In the ABSORB and SPIRIT trials, the mean acute recoil of the bioabsorbable everolimus-eluting coronary scaffold (Absorb BVS 1.0, Abbott; 6.85±6.96%) was slightly higher than that of the metallic everolimus-eluting stent (XIENCE V, Abbott; 4.27±7.08%)[24], and the improved Absorb BVS revision 1.1 had an acute recoil similar to that of the Absorb BVS revision 1.0[13]. In the present study, both the BRS and SES had similar acute recoil (2.50±7.33% vs 2.44±5.78%; p=0.97), which suggests that, like the commercially available SES, the BRS could provide sufficient radial strength to support a vessel wall in the acute phase. OCT analysis showed that the LA and SA of the stents in the BRS group were significantly smaller than those in the SES group at the 14-day and 28-day assessments but that there was no significant between-group difference in the NA. Therefore, consideration should be given to the possibility of late recoil with the BRS caused by a decrease in radial strength. However, at the 97-day and 189-day assessments, both OCT and the histopathological examination showed that the BRS scaffold beam remained intact. There was no significant between-group difference in the LA or SA, and even the above-mentioned parameters in the BRS group surpassed those in the SES group,

suggesting that the novel 3D-printed absorbable scaffold can provide enough support to resist elastic recoil and restrict neointimal proliferation in porcine coronary arteries for at least 6 months. This novel scaffold has a unique closed-loop unit structure with a spiral arrangement and is circular in cross-section, which is conducive to attachment to the inner wall of a blood vessel and reducing the effect on local blood flow[8]. Therefore, in theory, the novel scaffold could provide a better local haemodynamic microenvironment in treated vessels, thereby reducing the risk of ST. Furthermore, the novel nanoparticle coating on the scaffold effectively inhibits proliferation of smooth muscle cells *in vitro*[25]. This could be the reason for its good flexural properties, radial support force, and limited neointimal proliferation. However, the lack of immediate baseline OCT data in this study meant that it was not possible to analyse the late stent recoil, and this will be the subject of a future study.

An earlier study of the Absorb BVS in a porcine coronary model[26] showed late lumen gain with an increase in the LA of the BVS from 2.87 ± 1.28 mm^2 at 28 days to 5.13 ± 0.84 mm^2 at 2 years and 6.85 ± 1.25 mm^2 at 4 years. Serial assessment of this BVS in patients showed a similar tendency, with further intravascular ultrasound examination suggesting that reduction of plaque led to late lumen enlargement rather than positive vessel remodelling[27]. An earlier preclinical study demonstrated that this late lumen gain might be coupled with positive remodelling of the scaffold-treated segment[28]. In our study, late lumen enlargement and SA enlargement of the BRS were similarly documented by OCT. Analysis of the mean LA on OCT showed a significant increase from 2.93 ± 1.03 mm^2 at 28 days to 4.31 ± 1.06 mm^2 at 189 days and an increase in SA from 3.86 ± 0.98 mm^2 at 28 days to 5.89 ± 1.22 mm^2 at 189 days. However, the OCT was performed in different animals at each time point in this study; therefore, the late lumen enlargement might be a pseudomorph. Therefore, continuous intravascular imaging, such as continuous OCT or intravascular ultrasound follow-up studies, should be considered to validate this phenomenon. In addition, we will make more efforts to characterise the change in tissue composition during biodegradation by histopathology on the neointimal tissue around the struts in the long-term evaluation, per the European Society of Cardiology/European Association of Percutaneous Cardiovascular Interventions Task Force's executive summary on bioresorbable scaffolds[29].

Finally, the scaffold was manufactured by 3D printing technology and can be tailor-made for specific coronary lesions, to help prevent device-vessel mismatch and associated malapposition, and avoid incomplete coverage of lesions, stent overlap, and uncovered struts. Considering that this study primarily explored the safety of this novel scaffold in porcine coronary arteries, this potential advantage should be investigated in further preclinical and clinical studies.

Limitations

This study had some limitations. First, it was performed in healthy animals with no atherosclerotic lesions in the coronary arteries. Therefore, it could not reflect complex clinical scenarios. Moreover, the possibility that growth of the animals during the study contributed to positive vessel remodelling cannot be excluded. Second, different animal cohorts were examined at the different assessment times without the benefit of serial observations in the same animals. The late scaffold discontinuity and late recoil of BRS were two important influencing factors in determining late outcomes. A serial intravascular imaging study in the same vessels and long-term histopathological analysis would be needed to observe dynamic evolution. Third, we used only one size of stent and did not tailor the stent to fit the vessel in each animal. Therefore, this study did not fully reflect the characteristics of 3D printing technology, and further research is needed to explore personalised percutaneous coronary intervention based on intravascular imaging and 3D printing technology.

Conclusions

This novel 3D-printed BRS showed safety and efficacy similar to that of an SES in a porcine model and had a long-term positive remodelling effect. Our preliminary findings for this novel stent warrant further clinical evaluation in patients with coronary artery disease.

Impact on daily practice

This preclinical study validated the safety and efficacy of a fully degradable sirolimus-eluting 3D-printed scaffold by implanting it into normal coronary arteries in a porcine model. The scaffold could be tailor-made for specific coronary lesions, which could help to prevent device-vessel mismatch and associated malapposition, and avoid incomplete coverage of lesions, stent overlap, and uncovered struts. Ultimately it may reduce clinical events and improve patient outcomes.

Conflict of interest statement

The authors have no conflicts of interest to declare.

References

1. Ormiston JA, Serruys PW. Bioabsorbable coronary stents. *Circ Cardiovasc Interv.* 2009;2:255-60.

2. Serruys PW, Garcia-Garcia HM, Onuma Y. From metallic cages to transient bioresorbable scaffolds: change in paradigm of coronary revascularization in the upcoming decade? *Eur Heart J.* 2012;33:16-25b.

3. Garcia-Garcia HM, Serruys PW, Campos CM, Muramatsu T, Nakatani S, Zhang YJ, Onuma Y, Stone GW. Assessing bioresorbable coronary devices: methods and parameters. *JACC Cardiovasc Imaging.* 2014;7:1130-48.

4. Kereiakes DJ, Ellis SG, Metzger C, Caputo RP, Rizik DG, Teirstein PS, Litt MR, Kini A, Kabour A, Marx SO, Popma JJ, McGreevy R, Zhang Z, Simonton C, Stone GW; ABSORB III Investigators. 3-Year Clinical Outcomes With Everolimus-Eluting Bioresorbable Coronary Scaffolds: The ABSORB III Trial. *J Am Coll Cardiol.* 2017;70:2852-62.

5. Elias J, van Dongen IM, Kraak RP, Tijssen RYG, Claessen BEPM, Tijssen JGP, de Winter RJ, Piek JJ, Wykrzykowska JJ, Henriques JPS. Mid-term and long-term safety and efficacy of bioresorbable vascular scaffolds versus metallic everolimus-eluting stents in coronary artery disease: A weighted meta-analysis of seven randomised controlled trials including 5577 patients. *Neth Heart J.* 2017;25:429-38.

6. Sotomi Y, Suwannasom P, Serruys PW, Onuma Y. Possible mechanical causes of scaffold thrombosis: insights from case reports with intracoronary imaging. *EuroIntervention.* 2017;12:1747-56.

7. Jinnouchi H, Torii S, Sakamoto A, Kolodgie FD, Virmani R, Finn AV. Fully bioresorbable vascular scaffolds: lessons learned and future directions. *Nat Rev Cardiol.* 2019;16:286-304.

8. Tenekecioglu E, Torii R, Bourantas C, Sotomi Y, Cavalcante R, Zeng Y, Collet C, Crake T, Suwannasom P, Onuma Y, Serruys PW. Difference in haemodynamic microenvironment in vessels scaffolded with Absorb BVS and Mirage BRMS: insights from a preclinical endothelial shear stress study. *EuroIntervention.* 2017;13:1327-35.

9. Zhang LR, Xu DS, Liu XC, Wu XS, Ying YN, Dong Z, Sun FW, Yang PP, Li X. [Coronary artery lumen diameter and bifurcation angle derived from CT coronary angiographic image in healthy people] [Article in Chinese]. *Zhonghua Xin Xue Guan Bing Za Zhi.* 2011;39:1117-23.

10. Jinnouchi H, Sakakura K, Yanase T, Ugata Y, Tsukui T, Taniguchi Y, Yamamoto K, Seguchi M, Wada H, Fujita H. Impact of stent edge dissection detected by optical coherence tomography after current-generation drug-eluting stent implantation. *PLoS One.* 2021;16:e0259693.

11. Kobayashi N, Mintz GS, Witzenbichler B, Metzger DC, Rinaldi MJ, Duffy PL, Weisz G, Stuckey TD, Brodie BR, Parvataneni R, Kirtane AJ, Stone GW, Maehara A. Prevalence, Features, and Prognostic Importance of Edge Dissection After Drug-Eluting Stent Implantation: An ADAPT-DES Intravascular Ultrasound Substudy. *Circ Cardiovasc Interv.* 2016;9:e003553.

12. Zhang B, Chen M, Zheng B, Wang XG, Wang XT, Fan YY, Huo Y. A novel high nitrogen nickel-free coronary stents system: evaluation in a porcine model. *Biomed Environ Sci.* 2014;27:289-94.

13. Onuma Y, Serruys PW, Gomez J, de Bruyne B, Dudek D, Thuesen L, Smits P, Chevalier B, McClean D, Koolen J, Windecker S, Whitbourn R, Meredith I, Garcia-Garcia H, Ormiston JA; ABSORB Cohort A and B investigators. Comparison of in vivo acute stent recoil between the bioresorbable everolimus-eluting coronary scaffolds (revision 1.0 and 1.1) and the metallic everolimus-eluting stent. *Catheter Cardiovasc Interv.* 2011;78:3-12.

14. Tearney GJ, Regar E, Akasaka T, Adriaenssens T, Barlis P, Bezerra HG, Bouma B, Bruining N, Cho JM, Chowdhary S, Costa MA, de Silva R, Dijkstra J, Di Mario C, Dudek D, Falk E, Feldman MD, Fitzgerald P, Garcia-Garcia HM, Gonzalo N, Granada JF, Guagliumi G, Holm NR, Honda Y, Ikeno F, Kawasaki M, Kochman J, Koltowski L, Kubo T, Kume T, Kyono H, Lam CC, Lamouche G, Lee DP, Leon MB, Maehara A, Manfrini O, Mintz GS, Mizuno K, Morel MA, Nadkarni S, Okura H, Otake H, Pietrasik A, Prati F, Räber L, Radu MD, Rieber J, Riga M, Rollins A, Rosenberg M, Sirbu V, Serruys PW, Shimada K, Shinke T, Shite J, Siegel E, Sonoda S, Suter M, Takarada S, Tanaka A, Terashima M, Thim T, Uemura S, Ughi GJ, van Beusekom HM, van der Steen AF, van Es GA, van Soest G, Virmani R, Waxman S, Weissman NJ, Weisz G; International Working Group for Intravascular Optical Coherence Tomography (IWG-IVOCT). Consensus standards for acquisition, measurement, and reporting of intravascular optical coherence tomography studies: a report from the International Working Group for Intravascular Optical Coherence Tomography Standardization and Validation. *J Am Coll Cardiol.* 2012;59:1058-72.

15. Otsuka F, Pacheco E, Perkins LE, Lane JP, Wang Q, Kamberi M, Frie M, Wang J, Sakakura K, Yahagi K, Ladich E, Rapoza RJ, Kolodgie FD, Virmani R. Long-term

safety of an everolimus-eluting bioresorbable vascular scaffold and the cobalt-chromium XIENCE V stent in a porcine coronary artery model. *Circ Cardiovasc Interv.* 2014;7:330-42.

16. Schwartz RS, Huber KC, Murphy JG, Edwards WD, Camrud AR, Vlietstra RE, Holmes DR. Restenosis and the proportional neointimal response to coronary artery injury: results in a porcine model. *J Am Coll Cardiol.* 1992;19:267-74.

17. Khalaj R, Tabriz AG, Okereke MI, Douroumis D. 3D printing advances in the development of stents. *Int J Pharm.* 2021;609:121153.

18. Sang Jin Lee, Ha Hyeon Jo, Kyung Seob Lim, Dohyung Lim, Soojin Lee, Jun Hee Lee, Wan Doo Kim, Myung Ho Jeong, Joong Yeon Lim, Il Keun Kwon, Youngmee Jung, Jun-Kyu Park, Su A Park. Heparin coating on 3D printed poly (l-lactic acid) biodegradable cardiovascular stent via mild surface modification approach for coronary artery implantation. *Chem Engineering J.* 2019;378:122116.

19. Lincoff AM, Furst JG, Ellis SG, Tuch RJ, Topol EJ. Sustained local delivery of dexamethasone by a novel intravascular eluting stent to prevent restenosis in the porcine coronary injury model. *J Am Coll Cardiol.* 1997;29:808-16.

20. Yamawaki T, Shimokawa H, Kozai T, Miyata K, Higo T, Tanaka E, Egashira K, Shiraishi T, Tamai H, Igaki K, Takeshita A. Intramural delivery of a specific tyrosine kinase inhibitor with biodegradable stent suppresses the restenotic changes of the coronary artery in pigs in vivo. *J Am Coll Cardiol.* 1998;32:780-6.

21. Moncada S, Palmer RM, Higgs EA. Nitric oxide: physiology, pathophysiology, and pharmacology. *Pharmacol Rev.* 1991;43:109-42.

22. Yamamoto T, Shibata R, Ishii M, Kanemura N, Kito T, Suzuki H, Miyake H, Maeda K, Tanigawa T, Ouchi N, Murohara T. Therapeutic reendothelialization by induced pluripotent stem cells after vascular injury-brief report. *Arterioscler Thromb Vasc Biol.* 2013;33:2218-21.

23. Yin T, Du R, Wang Y, Huang J, Ge S, Huang Y, Tan Y, Liu Q, Chen Z, Feng H, Du J, Wang Y, Wang G. Two-stage degradation and novel functional endothelium characteristics of a 3-D printed bioresorbable scaffold. *Bioact Mater.* 2021;10:378-96.

24. Tanimoto S, Serruys PW, Thuesen L, Dudek D, de Bruyne B, Chevalier B, Ormiston JA. Comparison of in vivo acute stent recoil between the bioabsorbable everolimus-eluting coronary stent and the everolimus-eluting cobalt chromium coronary stent: insights from the ABSORB and SPIRIT trials. *Catheter Cardiovasc Interv.* 2007;70:515-23.

25. Zhao J, Mo Z, Guo F, Shi D, Han QQ, Liu Q. Drug loaded nanoparticle coating on totally bioresorbable PLLA stents to prevent in-stent restenosis. *J Biomed Mater Res B Appl Biomater.* 2018;106:88-95.

26. Onuma Y, Serruys PW, Perkins LE, Okamura T, Gonzalo N, García-García HM, Regar E, Kamberi M, Powers JC, Rapoza R, van Beusekom H, van der Giessen W, Virmani R. Intracoronary optical coherence tomography and histology at 1 month and 2, 3, and 4 years after implantation of everolimus-eluting bioresorbable vascular scaffolds in a porcine coronary artery model: an attempt to decipher the human optical coherence tomography images in the ABSORB trial. *Circulation.* 2010;122: 2288-300.

27. Serruys PW, Ormiston JA, Onuma Y, Regar E, Gonzalo N, Garcia-Garcia HM, Nieman K, Bruining N, Dorange C, Miquel-Hébert K, Veldhof S, Webster M, Thuesen L, Dudek D. A bioabsorbable everolimus-eluting coronary stent system (ABSORB): 2-year outcomes and results from multiple imaging methods. *Lancet.* 2009;373:897-910.

28. Strandberg E, Zeltinger J, Schulz DG, Kaluza GL. Late positive remodeling and late lumen gain contribute to vascular restoration by a non-drug eluting bioresorbable scaffold: a four-year intravascular ultrasound study in normal porcine coronary arteries. *Circ Cardiovasc Interv.* 2012;5:39-46.

29. Byrne RA, Stefanini GG, Capodanno D, Onuma Y, Baumbach A, Escaned J, Haude M, James S, Joner M, Jüni P, Kastrati A, Oktay S, Wijns W, Serruys PW, Windecker S. Report of an ESC-EAPCI Task Force on the evaluation and use of bioresorbable scaffolds for percutaneous coronary intervention: executive summary. *Eur Heart J.* 2018;39:1591-601.